Article:
Hollerbach, R and Khan, F (2016) Phase Slip Solutions in Magnetically Modulated Taylor-Couette Flow. Acta Mechanica, 227 (2). pp. 311-319. ISSN: 0001-5970

https://doi.org/10.1007/s00707-015-1447-7

Acta Mechanica manuscript No.
(will be inserted by the editor)

Rainer Hollerbach · Farzana Khan

Phase Slip Solutions in Magnetically Modulated Taylor-Couette Flow

Received: date / Accepted: date

Abstract We numerically investigate Taylor-Couette flow in a wide-gap configuration, with $r_i/r_o = 1/2$, the inner cylinder rotating, and the outer cylinder stationary. The fluid is taken to be electrically conducting, and a magnetic field of the form $B_z \approx (1 + \cos(2\pi z/z_0))/2$ is externally imposed, where the wavelength $z_0 = 50(r_o - r_i)$. Taylor vortices form where the field is weak, but not where it is strong. As the Reynolds number measuring the rotation rate is increased, the initial onset of vortices involves phase slip events, whereby pairs of Taylor vortices are periodically formed and then drift outward, away from the midplane where $B_z = 0$. Subsequent bifurcations lead to a variety of other solutions, including ones both symmetric and asymmetric about the midplane. For even larger Reynolds numbers a different type of phase slip arises, in which vortices form at the outer edges of the pattern and drift inward, disappearing abruptly at a certain point. These solutions can also be symmetric or asymmetric about the midplane, and co-exist at the same Reynolds number. Many of the dynamics of these phase slip solutions are qualitatively similar to previous results in geometrically ramped Taylor-Couette flows.

1 Introduction

The flow between differentially rotating cylinders, known as Taylor-Couette flow (TC flow), is one of the oldest problems in fluid dynamics, but continues to attract considerable experimental [1–3] as well as numerical [4–6] interest. Another indication of its continuing relevance is the number of distinct branches it has spawned. Two of these are: (a) ramped TC flow, where the inner and/or outer radii of the cylinders are not uniform, but vary along the axial direction, and (b) magnetic TC flow, where the fluid is taken to be electrically conducting, and magnetic fields are externally applied. In this work we combine these two branches, by using magnetic fields to impose the axial modulation that is otherwise created by the geometrical ramping. We demonstrate that the phenomenon of phase slip, whereby pairs of Taylor vortices are either created or destroyed, carries over from geometrically to magnetically ramped TC flows. We suggest that magnetically modulated TC flow may be a more convenient system to numerically study some of the resulting pattern formation effects.

The configuration of greatest interest in ramped TC flow is when the radii of the cylinders gradually vary in such a way that parts of the domain can be above the critical Reynolds number for the onset of Taylor vortices while other parts are still below. Refs. [7,8] considered such subcritical ramps in a general pattern formation context, and showed that the usual Eckhaus-stable wave-number band instead collapses to a single wave-number. Riecke & Paap [9] applied this so-called phase-diffusion

R. Hollerbach
Department of Applied Mathematics, University of Leeds, Leeds, LS2 9JT, UK
E-mail: rh@maths.leeds.ac.uk

F. Khan
Department of Applied Mathematics, University of Leeds, Leeds, LS2 9JT, UK
Permanent address: Department of Mathematics, Quaid-i-Azam University, Islamabad, Pakistan

equation approach specifically to TC flows, and demonstrated that "there exist ramps which do not permit any static patterns but force them to drift." That is, once the wave-number is fixed, at the transition point(s) from locally subcritical to supercritical, that can force the wave-number in other parts of the supercritical region to be Eckhaus-unstable. The pattern responds with a phase slip event, essentially an attempt to move the wave-number toward Eckhaus stability. The resulting Taylor vortices drift away though, forcing a new phase slip, and so on indefinitely. (Note however that not all subcritically ramped systems necessarily lead to phase slip behaviour; for reviews of various pattern-forming systems without phase slip see [10].)

Occurring in parallel with the theory of Riecke & Paap were a series of experiments [11–13] which confirmed many of these ideas, including the uniqueness of the selected wave-number and the possibility of drifting patterns. Paap & Riecke [14] in turn followed up with further work demonstrating that the phase equation approach yields quantitatively accurate agreement with many of these experimental results. They further suggested that it should be possible to construct ramps where the phase slip events occur irregularly, resulting in spatiotemporal chaos in the pattern. Ref. [15] took up this challenge experimentally, and succeeded in obtaining a period-doubling cascade to chaotic phase dynamics. We therefore conclude our overview of ramped TC flow by noting that there is a broad variety of possible patterns, and a good theoretical framework for understanding many of these results.

Turning next to magnetic TC flow, the current focus of attention is primarily on the magnetorotational instability (MRI), whereby a magnetic field can destabilize a rotation profile that would otherwise be stable according to the Rayleigh criterion. First discovered in 1959 in TC flows [16], the MRI lay largely dormant until it was suggested that it might play a crucial role in astrophysical accretion disks [17]. This discovery reignited interest in the MRI in TC flows, and specifically the possibility of obtaining it [18,19] or variants of it [20,21] experimentally. The standard MRI has not yet been obtained [22,23], but the helical [24] and azimuthal [25] variants have. A further recent magnetic TC experiment [26] has measured the so-called ω-effect.

However, here we wish to return to some of the earliest work [27–29] on magnetic TC flows, dating back over 50 years. In the standard configuration where the outer cylinder is stationary (and the Rayleigh criterion therefore does not enforce hydrodynamic stability), both theory [27] and experiment [28,29] agree that imposing a uniform axial magnetic field has a stabilizing influence, that is, delays the onset of Taylor vortices to greater Reynolds numbers. It is this stabilizing feature that forms the basis of our work here. In particular, suppose one were to impose not a uniform axial field, but instead $B_z \approx (1+\cos(2\pi z/z_0))/2$ [the precise form is given below in Eq. (3)]. That is, the field reaches a maximum at integer multiples of the basic periodicity z_0, and drops to zero at half-integer multiples of z_0. We would then expect to obtain Taylor vortices where the field is weak, and no Taylor vortices where it is strong – the same subcritical ramping effect as before in the geometrically ramped problem.

2 Equations

We consider the standard wide-gap Taylor-Couette configuration with radii r_i and r_o satisfying $r_i/r_o = 1/2$. The inner cylinder rotates at a rate Ω, and the outer cylinder is stationary. In the so-called inductionless limit, the suitably scaled Navier-Stokes and magnetic induction equations become

$$Re\frac{\partial \mathbf{U}}{\partial t} = -\nabla p + \nabla^2\mathbf{U} - Re\mathbf{U}\cdot\nabla\mathbf{U} + Ha^2(\nabla\times\mathbf{b})\times\mathbf{B}_0, \tag{1}$$

$$\nabla^2\mathbf{b} = -\nabla\times(\mathbf{U}\times\mathbf{B}_0). \tag{2}$$

Length has been scaled by r_i, time by Ω^{-1}, and $\mathbf{U}$ by Ωr_i. $\mathbf{B}_0$ is the externally imposed magnetic field, and $\mathbf{b}$ the induced field. The two nondimensional parameters in these equations are the usual Reynolds number

$$Re = \frac{\Omega r_i^2}{\nu}$$

measuring the inner cylinder's rotation rate, and the Hartmann number

$$Ha = \frac{B_0 r_i}{\sqrt{\mu\rho\nu\eta}}$$

measuring the strength of the imposed field. The quantities μ, ρ, ν, and η are the fluid's permeability, density, viscosity, and magnetic diffusivity, respectively. See also [30,31] for a more detailed derivation of these equations in the inductionless limit, in the context of magnetic spherical Couette flow. For experiments in magnetic spherical Couette flow see [32,33] and further references therein.

The spatial structure of the imposed field $\mathbf{B}_0$ is given by

$$\mathbf{B}_0 = \left[(1+\cos(\kappa z)I_0(\kappa r))/2\right]\hat{\mathbf{e}}_z + \left[\sin(\kappa z)I_1(\kappa r)/2\right]\hat{\mathbf{e}}_r, \tag{3}$$

where $\kappa = 2\pi/z_0$, and I_0 and I_1 are the modified Bessel functions [34]. The wavelength z_0 is an adjustable parameter, but once fixed, the rest of the structure is completely determined by the requirements that $\mathbf{B}_0$ be a potential field, and imposed from the region $r > r_o$ rather than $r < r_i$. That is, with a suitable array of external Helmholtz coils one could actually impose such a field, a point we will return to in the conclusion. Note finally that the r-dependent parts of $\mathbf{B}_0$ are necessary to satisfy $\nabla \cdot \mathbf{B}_0 = 0$ and $\nabla \times \mathbf{B}_0 = \mathbf{0}$, but are in fact quite small. Using the asymptotic properties $I_0(\kappa r) \approx 1$ and $I_1(\kappa r) \ll 1$ for $\kappa r \ll 1$, one obtains $\mathbf{B}_0 \approx [(1+\cos(\kappa z))/2]\,\hat{\mathbf{e}}_z$, as desired to create the magnetic ramping effect.

These equations (1-3), together with boundary conditions no-slip for $\mathbf{U}$ and perfectly conducting for $\mathbf{b}$, were numerically solved using an axisymmetric, pseudo-spectral code [35]. Very briefly, $\mathbf{U}$ and $\mathbf{b}$ are expanded as

$$\mathbf{U} = \nabla \times (\psi\,\hat{\mathbf{e}}_\phi) + v\,\hat{\mathbf{e}}_\phi, \qquad \mathbf{b} = \nabla \times (a\,\hat{\mathbf{e}}_\phi) + b\,\hat{\mathbf{e}}_\phi,$$

then ψ, v, a and b are further expanded in terms of Chebyshev polynomials in r and Fourier series in z. Typical resolutions used were $20-30$ Chebyshev polynomials and $200-300$ Fourier modes. The time-stepping of Eq. (1) is second-order Runge-Kutta, modified to treat the diffusive terms implicitly. Eq. (2) is directly inverted for $\mathbf{b}$ at each time-step of Eq. (1). Typical time-steps used were $0.02-0.05$.

After preliminary scans in the range $z_0 = 20-80$ yielded qualitatively similar phase slip solutions, the axial length was fixed at $z_0 = 50$. For comparison, the spatially ramped experiment [15] most closely related to our magnetic case had a nondimensional length of 29. Again after some preliminary scans, it was found that Hartmann numbers in the range $2-10$ also yielded similar solutions, so only $Ha = 5$ was investigated in further detail. The single remaining parameter, the Reynolds number, was then varied throughout the interval $Re = 67-85$. The reason for the lower limit is simple: in the non-magnetic problem the critical Reynolds number for the onset of Taylor vortices is known [36] to be 68.2, so one would hardly expect anything interesting to happen before then in this problem. The upper limit was chosen partly because enough interesting things had already happened by then, and partly because the calculations become more time-consuming beyond that point. Eventually of course one would also expect the solutions to become three-dimensional, although in the non-magnetic problem at least non-axisymmetric instabilities do not arise until much larger Reynolds numbers, around three times supercritical [37] versus less than 30% supercriticality considered here.

Finally, it is worth noting that at least some of the cases required extremely long integration times before periodic solutions emerged. This is a natural consequence of having $z_0 \gg 1$: the diffusive time-scale between two points separated by the maximum possible distance $z_0/2$ is $Re(z_0/2)^2 = O(10^5)$, so very long time-scales are almost inevitable.

3 Results

Figure 1 shows the flow at $Re = 67$, still below the onset of Taylor vortices. There is in fact already a deviation from the ideal Couette profile, most noticeably in the meridional circulation ψ, which is identically zero in the ideal basic state, but now consists of four large circulation cells centered on the midplane $z = 25$. These cells already appear for all $Re > 0$, and are analogous to the Ekman cells obtained in cylinders with top and bottom endplates [12,38]. In this case they are caused by the r-dependent parts of $\mathbf{B}_0$; if the imposed field were exactly $B_z = (1+\cos(\kappa z))/2$, then the ideal Couette profile $v = C_1 r + C_2/r$ would also be an exact solution of the Navier-Stokes equation, along with $\psi = 0$. By taking z_0 to be sufficiently large, these deviations from the ideal profile can thus be made as small as desired. Geometrically ramped TC flows also have deviations from the ideal Couette profile, caused by similar dynamics as the endplate-induced Ekman cells. These deviations from the ideal profile are not crucial though to any of the phase equation results, including the existence of drifting patterns [9].

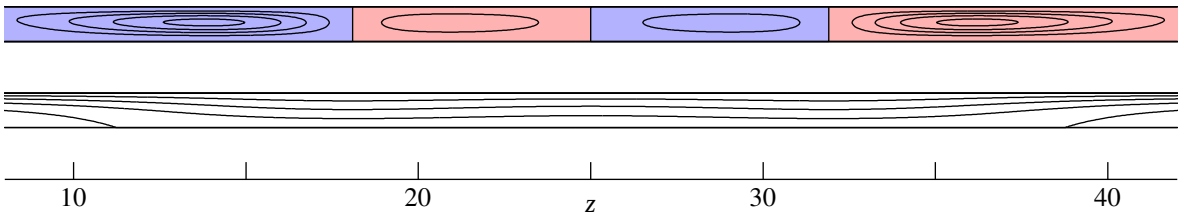

Fig. 1 The solution at $Re = 67$. The top row shows the meridional circulation ψ, with a contour interval of 10^{-3}, and blue/red indicating clockwise/counter-clockwise circulation. The second row shows v, with a contour interval of 0.25. The horizontal axis corresponds to length z along the cylinders; the regions $z < 8$ and $z > 42$ are not shown as all the relevant dynamics occur in the middle region. On the vertical axis r_i is on the top and r_o is on the bottom.

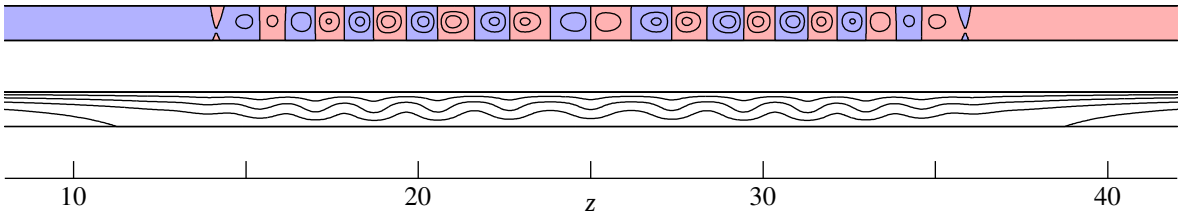

Fig. 2 The solution at $Re = 77$. The contour interval for ψ is now 0.01; everything else is as in figure 1. Note the Taylor vortices between $z \approx 14$ and 36, in the region where the field is weak. Based on the local value of the field, the flow should be linearly unstable to Taylor vortices in the region $13 < z < 37$, in excellent agreement.

Figure 2 shows the flow at $Re = 77$. As expected, we find Taylor vortices in the middle, where the imposed field is weak, but not near the ends, where it is strong. This solution is in fact steady, without either drift or phase slip events. However, it is also not the initial onset of Taylor vortices; instead, these solutions exist only in the range $76.5 < Re \leq 81.3$. Note how much stronger the meridional circulation in the Taylor vortices is, in comparison with the background cells from figure 1. This background circulation is still present even here, but is overwhelmed by the Taylor vortices, with the result that clockwise and counter-clockwise vortices are almost the same strength.

If figure 2 does not represent the initial onset, then at what Reynolds number do the Taylor vortices first arise, and how? The bifurcation point occurs at $Re = 67.4$, via a supercritical Hopf bifurcation, that is, a drifting pattern. Two further comments are also in order regarding this initial bifurcation. First, the slight reduction from 68.2 in the non-magnetic case [36] to 67.4 here is caused by the presence of the background cells, and does not indicate a subcritical bifurcation. Second, as a transition from a steady to a periodic solution, it is a true bifurcation. This is different from TC flows with endplates, where the background Ekman cells cause the bifurcation to be imperfect [39], from one steady pattern to another, but without any true bifurcation.

To best illustrate the full time-dependence of the drifting pattern, including the phase slip events that form a crucial part of it, we begin by noting that the radial structure of the vortices is relatively straightforward: $\psi = 0$ at either boundary, and in between is positive/negative for clockwise/counter-clockwise vortices. Simply focusing on the middle $r = 1.5$ will therefore capture all the essential features. Contour plots of $\psi(t, z, 1.5)$ will then reveal the structure in both time and length along the cylinder.

As illustrated in figure 3, the solution consists of a series of phase slips at the midplane $z = 25$. The newly created Taylor vortices drift outward, eventually fading away at $|z-25| \approx 10$, where the magnetic field becomes too strong for them to persist. Note also the slight asymmetry between the two phase slip events that constitute one period of the pattern. This is again caused by the weak background circulation; newly created vortices with circulation in the opposite sense as the background (figure 1) persist slightly longer than vortices with circulation in the same sense. The period of these solutions gradually increases from $T = 1243$ at $Re = 67.4$ to $T = 4393$ at $Re = 74.5$, the value shown in figure 3.

The next two bifurcations occur at $Re = 74.8$ and $Re = 75.8$. The first one breaks the midplane symmetry $\psi(t, z) = -\psi(t, 50 - z)$ seen in figure 3, but still preserves the shift-and-reflect symmetry

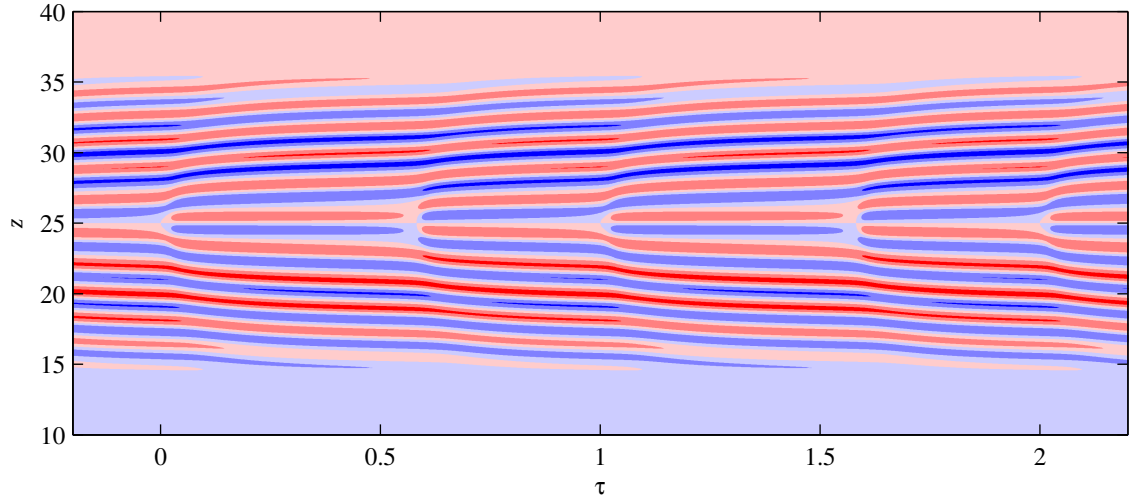

Fig. 3 Contour plots of $\psi(t, z, 1.5)$ at $Re = 74.5$, with a contour interval of 0.01. Blue/red represents clockwise/counter-clockwise Taylor vortices. On the horizontal axis $\tau = t/T$, where the period $T = 4393$ at this Reynolds number. Note the midplane symmetry $\psi(t, z) = -\psi(t, 50 - z)$, and the slightly uneven timing between the two phase slips per period.

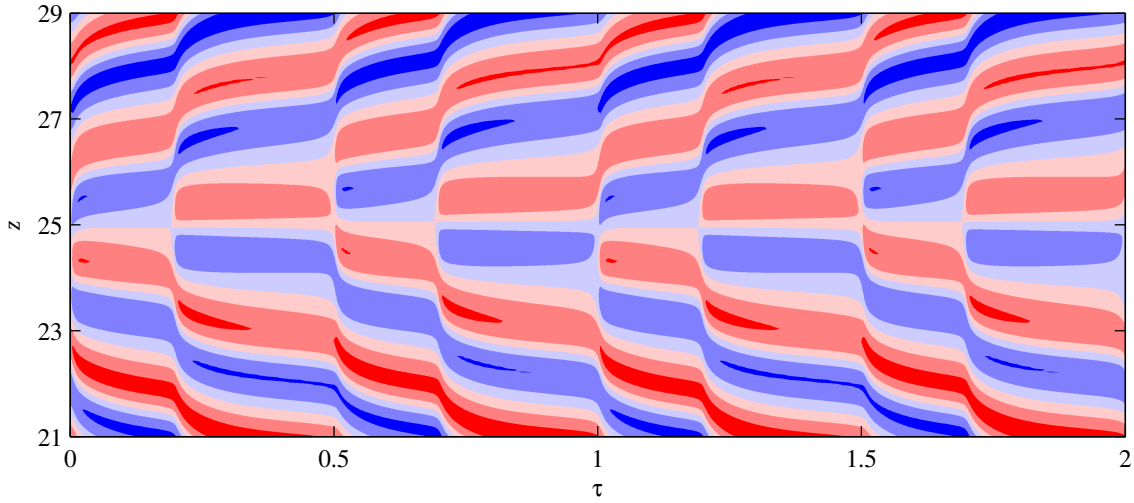

Fig. 4 As in figure 3, but at $Re = 75.5$, where the period $T = 13334$. Note the shift-and-reflect symmetry $\psi(t, z) = -\psi(t + T/2, 50 - z)$, and the four phase slips per period.

$\psi(t, z) = -\psi(t + T/2, 50 - z)$. Correspondingly, the average value of the asymmetric component over a period is still zero. The second one breaks the shift-and-reflect symmetry as well. There are thus two solutions, with average asymmetric components of either sign (just as in a pitchfork bifurcation). Figures 4 and 5 show examples of these solutions, at $Re = 75.5$ and $Re = 76$. The first bifurcation already causes the period to double, since it now takes two of the original cycles for the asymmetry to occur first in one half and then in the other. Beyond that, the periods still continue increasing, from $T = 13334$ at $Re = 75.5$ to $T = 22616$ at $Re = 76$. Both of these symmetry-breaking bifurcations are also supercritical, with no hysteresis if Re is reduced again.

Figure 6 shows the pattern at $Re = 76.5$. We notice two differences in comparison with figure 5. First, the asymmetry is considerably greater, with the pattern shifted so much in z that there is now a Taylor vortex sitting right on the midpoint $z = 25$. Figure 7 compares the entire range $67 \le Re \le 77$, and quantifies items such as how the strength of the Taylor vortices gradually increases, how the degree of asymmetry increases, and how the period varies.

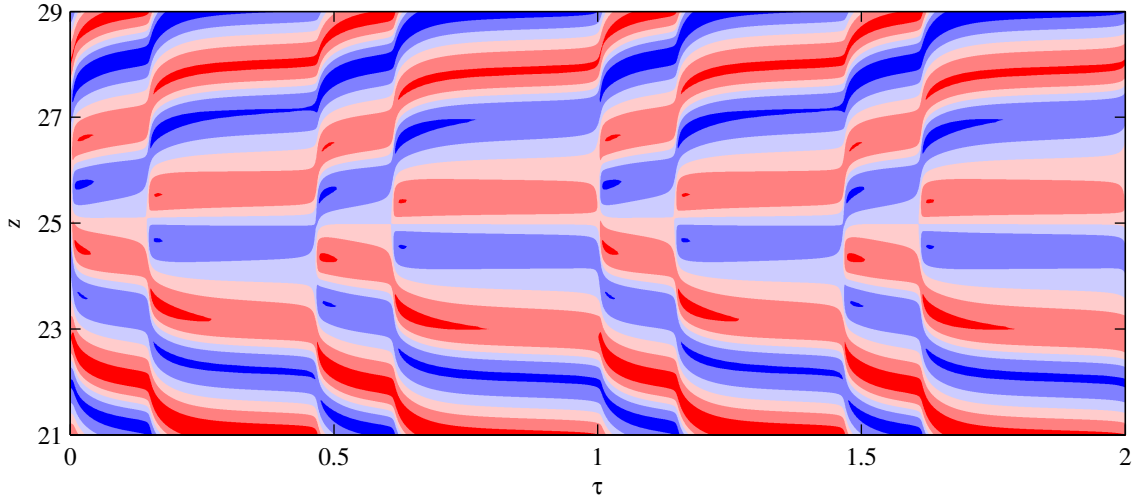

Fig. 5 As in figure 3, but at $Re = 76$, where the period $T = 22616$. Note the four phase slips per period, and the uneven timing between successive pairs; this is the most obvious manifestation of the loss of the previous shift-and-reflect symmetry in figure 4.

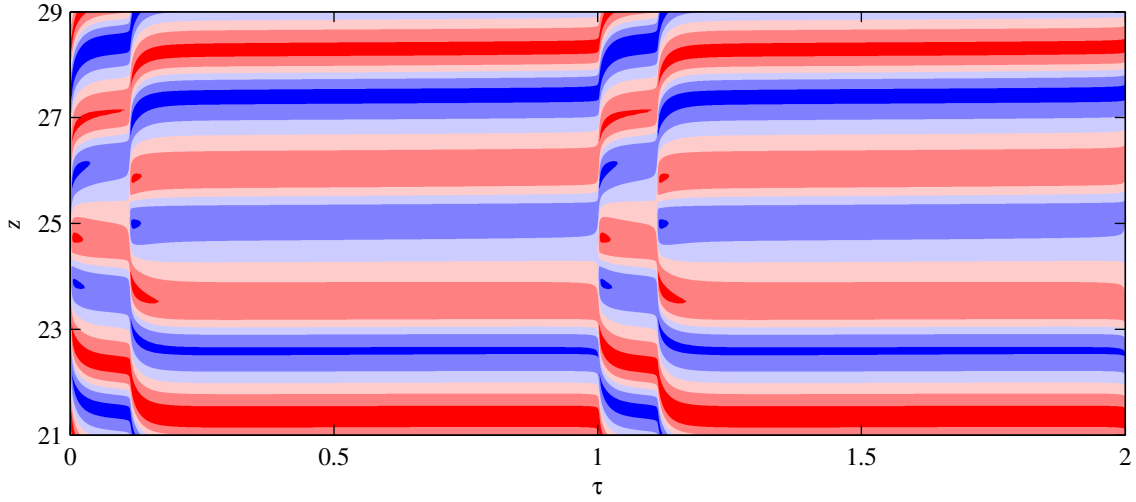

Fig. 6 As in figure 3, but at $Re = 76.5$, where the period $T = 54388$. Note the two phase slips per period, and the extreme disparity in timing between the two, with the pattern almost stationary for most of the cycle.

The second difference is that the pattern in figure 6 has only two phase slip events per period, whereas in figure 5 there are four per period. The most natural way to connect the two therefore would be to have a period-doubling bifurcation as Re is reduced from 76.5 back toward 76. Pinning down exactly where this bifurcation occurs was unfortunately not possible. For $Re \leq 76.05$ the solutions have four phase slips per period, and for $Re \geq 76.25$ they have two per period. However, between 76.05 and 76.25 they not only have very long cycle times (see figure 7), but even after integrating to $t = 10^6$ the solutions still had not settled in to a precise periodicity. It is possible of course that the solutions in this narrow gap really are chaotic, and bifurcate to a four-cycle at one end and a two-cycle at the other.

Increasing Re even further, the pattern in figure 6 persists up to $Re = 76.63$, where a turning point is reached, and the solution collapses back to the steady, symmetric state as in figure 2. Reducing Re again, the figure 2 solutions become unstable to a subcritical pitchfork bifurcation at $Re = 76.53$. There is thus a small but measurable degree of hysteresis in this transition. Somewhere on the unstable

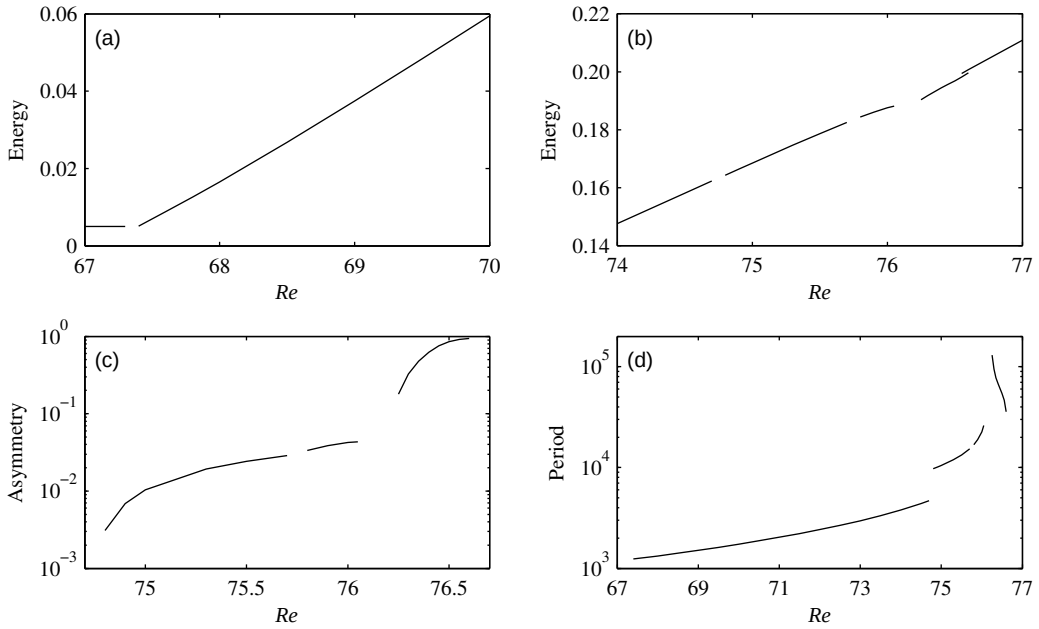

Fig. 7 Panels (a) and (b) both show the kinetic energy in the meridional circulation (period-averaged for the time-dependent solutions). Note how the energy is essentially constant before the onset of Taylor vortices, and increases linearly thereafter (including in the gap $70 < Re < 74$ between the two panels). Panel (c) shows the fraction of the energy that is contained in the asymmetric component. Note how it increases from 0 for $Re < 74.8$ toward almost 1 at the turning point $Re = 76.6$. Panel (d) shows the period; note the extreme variation over more than two orders of magnitude. Different line segments correspond to the different types of solutions discussed in the text.

branch between 76.53 and 76.63 the solution presumably also undergoes a Hopf bifurcation, thereby acquiring the time-dependence that it has in the figure 6 solutions.

Finally, on the steady, symmetric figure 2 branch, what happens if Re is increased rather than decreased? At $Re = 81.4$ a Hopf bifurcation occurs, or rather two essentially simultaneously, corresponding to symmetric and asymmetric perturbations. As a result, attempting to unravel the full details of the bifurcation diagram proved fruitless. The underlying dynamics are quite straightforward though. Figures 8 and 9 show two solutions that both exist at $Re = 85$. We note first that they are very different from the previous phase slip solutions. Rather than having pairs of vortices created in the middle and then drifting outward, we now have vortices moving in from the edges, and then being abruptly destroyed when $|z - 25|$ is around 8 or 9. Based on the local value of the field, the flow should be linearly unstable to Taylor vortices in the region $11 < z < 39$. All of these dynamics are thus happening within the expected region, but it is not clear what singles out the particular location where the phase slips occur.

Comparing figures 8 and 9, the most obvious difference between them is that figure 8 is symmetric, whereas figure 9 is asymmetric. That is, in figure 8 the phase slips in the top and bottom halves are in phase in time, whereas in figure 9 they are exactly half a period out of phase. This pattern presumably also explains why the two perturbation types both arose at virtually the same critical Reynolds number: If the two time-dependent regions are separated in space by such a large region that is essentially stationary, then the coupling between them is extremely weak, so there is almost nothing to fix their relative phases in time. This very weak coupling between the two regions also means that very long runs were required in some cases before a definite phase relationship emerged. Indeed, there may also be some Reynolds numbers where no definite relationship ever arises, resulting in some type of quasi-periodic solution. It is difficulties like these that lead us to concentrate on the single value $Re = 85$, rather than attempt to map out a full bifurcation diagram over the range $Re \geq 81.4$.

One further, not quite so obvious difference between figures 8 and 9 is revealed by counting the number of vortices in the stationary region, between the phase slip events. In figure 8 there are 18, in figure 9 only 16. The easiest way to spot that the number is certainly different is simply to note

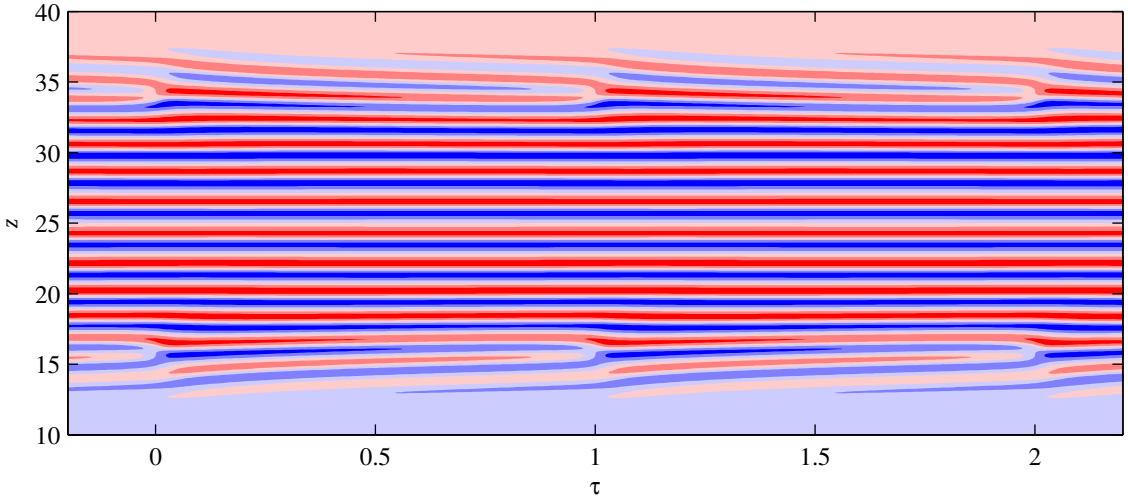

Fig. 8 One possible solution at $Re = 85$, with $T = 638$. Note the midplane symmetry, and the 18 essentially steady Taylor vortices separating the two time-dependent regions. The contour interval is 0.012.

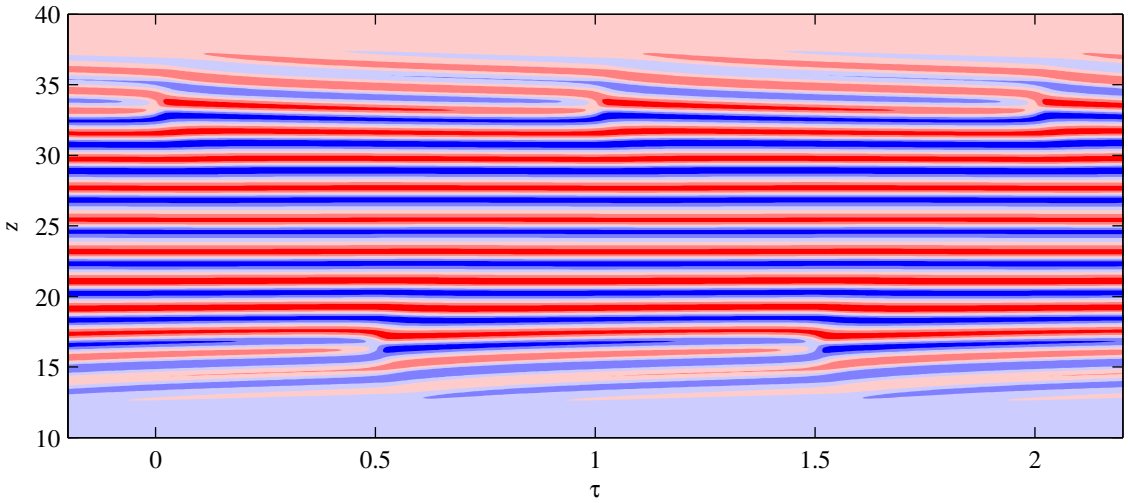

Fig. 9 Another solution at $Re = 85$, with $T = 755$. Note the shift-and-reflect symmetry, and the 16 essentially steady Taylor vortices separating the two time-dependent regions. The contour interval is 0.012.

that the coloring just above/below $z = 25$ is blue/red in figure 8, but red/blue in figure 9. These particular solutions were obtained by starting from a number of different, essentially random initial conditions. Motivated by these results though, one obvious question to ask would be: do there exist symmetric solutions with 16 vortices, and/or asymmetric solutions with 18 vortices? Various plausible initial conditions were therefore constructed, but all attempts invariably equilibrated back to either of figures 8 or 9.

4 Conclusion

We have seen in this work how a magnetically ramped Taylor-Couette system can yield qualitatively similar phase slip dynamics as in the more familiar geometrically ramped system. It would be of considerable interest to make the comparison more quantitative, by deriving the equivalent of the Riecke & Paap [9] phase-diffusion equation, and seeing whether it can indeed explain the results presented here. An analysis of the numerically computed wave-numbers unfortunately proved inconclusive; the

results never vary by more than a few percent from the expected non-magnetic values. Note for example how all the bands in figures 3, 8 and 9 have essentially the same axial extent, corresponding to round Taylor vortices. It is thus not entirely clear why our solutions exhibit phase slip at all, let alone two different types, occurring in different locations. A weakly nonlinear analysis as in other pattern-forming systems [10] might also be fruitful.

Future numerical extensions of this work include a systematic search for the spatiotemporal chaos predicted by Paap & Riecke [14]. This will likely require imposing fields consisting of harmonics κ, 2κ, etc., analogous to the special choices of ramps needed in the Paap & Riecke formulation. Also of interest is the magnetorotational instability mentioned in the introduction, where the magnetic field has a destabilizing rather than stabilizing influence; we would then expect to find Taylor vortices where the field is strong rather than weak.

More generally, it is noteworthy that there do not appear to be any direct numerical simulations of any of the geometrically ramped experiments mentioned in the introduction. The only related numerical work is [40], who did not address subcritical ramping though; instead they considered a scenario where the radii of the cylinders vary along the length, but in such a way that the onset of Taylor vortices still occurs simultaneously everywhere. This configuration yields vortices that form at one end and monotonically drift toward the other, but without any bifurcations beyond the initial transition from steady to periodic flows.

The most likely reason for this almost complete absence of numerical work in geometrically ramped TC flows is that the geometry then becomes too complicated to allow the very long integration times that are required for equilibrated solutions to emerge. In contrast, by keeping the geometry simple, in this work we were able to exploit efficient pseudo-spectral numerical methods that do allow very long integration times. We suggest therefore that for numerical studies of general pattern formation effects the magnetically ramped problem is more convenient.

Finally, it would be of great interest to see actual experiments done on this problem. Imposing magnetic fields as in Eq. (3) would be straightforward, simply by a suitable array of periodically spaced external Helmholtz coils. The required field strengths are also easily achievable; the existing PROMISE experiment [24, 25] already operates at slightly larger Hartmann numbers. The main difficulty would most likely be that the Reynolds numbers here are considerably lower than in the PROMISE experiment, where they are $O(10^3)$. The entire flow velocities are then also reduced, which could make them difficult to measure with the techniques commonly used in liquid metal experiments of this type [41, 42]. If these difficulties could be overcome though, then magnetically modulated Taylor-Couette flows would undoubtedly offer a rich variety of phenomena to study experimentally.

Acknowledgements RH was supported by STFC grant ST/K000853/1. FK's visit to the United Kingdom was supported by the Higher Education Commission of Pakistan.

References

1. van Gils, D.P.M., Bruggert, G.W., Lathrop, D.P., Sun, C., Lohse, D.: The Twente turbulent Taylor-Couette (T^3C) facility: Strongly turbulent (multiphase) flow between two independently rotating cylinders. Rev. Sci. Inst. **82**, 025105 (2011)
2. Avila, K., Hof, B.: High-precision Taylor-Couette experiment to study subcritical transitions and the role of boundary conditions and size effects. Rev. Sci. Inst. **84**, 065106 (2013)
3. Collins, C., Clark, M., Cooper, C.M., Flanagan, K., Khalzov, I.V., Nornberg, M.D., Seidlitz, B., Wallace, J., Forest, C.B.: Taylor-Couette flow of unmagnetized plasma. Phys. Plasmas **21**, 042117 (2014)
4. Youd, A.J., Willis, A.P., Barenghi, C.F.: Non-reversing modulated Taylor-Couette flows. Fluid Dyn. Res. **36**, 61–73 (2005)
5. Watanabe, T., Toya, Y.: Vertical Taylor-Couette flow with free surface at small aspect ratio. Acta Mech. **223**, 347–353 (2012)
6. Shi, L., Rampp, M., Hof, B., Avila, M.: A hybrid MPI-OpenMP parallel implementation for pseudospectral simulations with application to Taylor-Couette flow. Comp. Fluids **106**, 1–11 (2015)
7. Pomeau, Y., Manneville, P.: Stability and fluctuations of a spatially periodic convective flow. J. Phys. Paris **40**, L609–612 (1979)
8. Kramer, L., Ben-Jacob, E., Brand, H., Cross, M.C.: Wavelength selection in systems far from equilibrium. Phys. Rev. Lett. **49**, 1891–1894 (1982)
9. Riecke, H., Paap, H.-G.: Perfect wave-number selection and drifting patterns in ramped Taylor vortex flow. Phys. Rev. Lett. **59**, 2570–2573 (1987)

10. Chomaz, J.-M.: Global instabilities in spatially developing flows: non-normality and nonlinearity. Ann. Rev. Fluid Mech. **37**, 357–392 (2005)
11. Cannell, D.S., Dominguez-Lerma, M.A., Ahlers, G.: Experiments on wave number selection in rotating Couette-Taylor flow. Phys. Rev. Lett. **50**, 1365–1368 (1983)
12. Dominguez-Lerma, M.A., Cannell, D.S., Ahlers, G.: Eckhaus boundary and wave-number selection in rotating Couette-Taylor flow. Phys. Rev. A **34**, 4956–4970 (1986)
13. Ning, L., Ahlers, G., Cannell, D.S.: Wave-number selection and traveling vortex waves in spatially ramped Taylor-Couette flow. Phys. Rev. Lett. **64**, 1235–1238 (1990)
14. Paap, H.-G., Riecke, H.: Drifting vortices in ramped Taylor vortex flow: Quantitative results from phase equation. Phys. Fluids **3**, 1519–1532 (1991)
15. Wiener, R.J., Snyder, G.L., Prange, M.P., Frediani, D., Diaz, P.R.: Period-doubling cascade to chaotic phase dynamics in Taylor vortex flow with hourglass geometry. Phys. Rev. E **55**, 5489–5497 (1997)
16. Velikhov, E.P.: Stability of an ideally conducting liquid flowing between cylinders rotating in a magnetic field. Sov. Phys. JETP **9**, 995–998 (1959)
17. Balbus, S.A., Hawley, J.F.: A powerful local shear instability in weakly magnetized disks. Astrophys. J. **376**, 214–222 (1991)
18. Ji, H., Goodman, J., Kageyama, A.: Magnetorotational instability in a rotating liquid metal annulus. Mon. Not. Roy. Astron. Soc. **325**, L1–5 (2001)
19. Rüdiger, G., Zhang, Y.: MHD instability in differentially-rotating cylindric flows. Astron. Astrophys. **378**, 302–308 (2001)
20. Hollerbach, R., Rüdiger, G.: New type of magnetorotational instability in cylindrical Taylor-Couette flow. Phys. Rev. Lett. **95**, 124501 (2005)
21. Hollerbach, R., Teeluck, V., Rüdiger, G.: Nonaxisymmetric magnetorotational instabilities in cylindrical Taylor-Couette flow. Phys. Rev. Lett. **104**, 044502 (2010)
22. Nornberg, M.D., Ji, H., Schartman, E., Roach, A., Goodman, J.: Observation of magnetocoriolis waves in a liquid metal Taylor-Couette experiment. Phys. Rev. Lett. **104**, 074501 (2010)
23. Roach, A.H., Spence, E.J., Gissinger, C., Edlund, E.M., Sloboda, P., Goodman, J., Ji, H.: Observation of a free Shercliff layer instability in cylindrical geometry. Phys. Rev. Lett. **108**, 154502 (2012)
24. Stefani, F., Gundrum, T., Gerbeth, G., Rüdiger, G., Schultz, M., Szklarski, J., Hollerbach, R.: Experimental evidence for magnetorotational instability in a Taylor-Couette flow under the influence of a helical magnetic field. Phys. Rev. Lett. **97**, 184502 (2006)
25. Seilmayer, M., Galindo, V., Gerbeth, G., Gundrum, T., Stefani, F., Gellert, M., Rüdiger, G., Schultz, M., Hollerbach, R.: Experimental evidence for nonaxisymmetric magnetorotational instability in a rotating liquid metal exposed to an azimuthal magnetic field. Phys. Rev. Lett. **113**, 024505 (2014)
26. Colgate, S.A., Beckley, H., Si, J., Martinic, J., Westphahl, D., Slutz, J., Westrom, C., Klein, B., Schendel, P., Scharle, C., McKinney, T., Ginanni, R., Bentley, I., Mickey, T., Ferrel, R., Li, H., Pariev, V., Finn, J.: High magnetic shear gain in a liquid sodium stable Couette flow experiment: A prelude to an $\alpha - \Omega$ dynamo. Phys. Rev. Lett. **106**, 175003 (2011)
27. Chandrasekhar, S.: The stability of viscous flow between rotating cylinders in the presence of a magnetic field. Proc. Roy. Soc. A **216**, 293–309 (1953)
28. Donnelly, R.J., Ozima, M.: Hydromagnetic stability of flow between rotating cylinders. Phys. Rev. Lett. **4**, 497–498 (1960)
29. Donnelly, R.J., Ozima, M.: Experiments on stability of flow between rotating cylinders in presence of a magnetic field. Proc. Roy. Soc. A **266**, 272–286 (1962)
30. Hollerbach, R.: Non-axisymmetric instabilities in magnetic spherical Couette flow. Proc. Roy. Soc. A **465**, 2003–2013 (2009)
31. Travnikov, V., Eckert, K., Odenbach, S.: Influence of an axial magnetic field on the stability of spherical Couette flows with different gap widths. Acta Mech. **219**, 255–268 (2011)
32. Cabanes, S., Schaeffer, N., Nataf, H.-C.: Turbulence reduces magnetic diffusivity in a liquid sodium experiment. Phys. Rev. Lett. **113**, 184501 (2014)
33. Zimmermann, D.S., Triana, S.A., Nataf, H.-C., Lathrop, D.P.: A turbulent high magnetic Reynolds number experimental model of Earth's core. J. Geophys. Res. **119**, 4538–4557 (2014)
34. Abramowitz, M., Stegun, I.A.: Handbook of Mathematical Functions. Dover (1968)
35. Hollerbach, R.: Spectral solutions of the MHD equations in cylindrical geometry. Int. J. Pure Appl. Math. **42**, 575–581 (2008)
36. Dominguez-Lerma, M.A., Ahlers, G., Cannell, D.S.: Marginal stability curve and linear growth rate for rotating Couette-Taylor flow and Rayleigh-Bénard convection. Phys. Fluids **27**, 856–860 (1984)
37. Jones, C.A.: The transition to wavy Taylor vortices. J. Fluid Mech. **157**, 135–162 (1985)
38. Graham, R., Domaradzki, J.A.: Local amplitude equation of Taylor vortices and its boundary condition. Phys. Rev. A **26**, 1572–1579 (1982)
39. Rucklidge, A.M., Champneys, A.R.: Boundary effects and the onset of Taylor vortices. Physica D 191, 282–296 (2004)
40. Sprague, M.A., Weidman, P.D.: Continuously tailored Taylor vortices. Phys. Fluids **21**, 114106 (2009)
41. Cramer, A., Eckert, S., Gerbeth, G.: Flow measurements in liquid metals by means of the ultrasonic Doppler method and local potential probes. Eur. Phys. J. Special Topics **220**, 25–41 (2013)
42. Pulugundla, G., Heinicke, C., Karcher, C., Thess, A.: Lorentz force velocimetry with a small permanent magnet. Eur. J. Mech. B **41**, 23–28 (2013)